Orbital Angular Momentum with Index Modulation

Ertugrul Basar, *Senior Member, IEEE*

***Abstract*—Orbital angular momentum (OAM)-based mode division multiplexing (MDM) is an emerging physical layer solution for short-distance line-of-sight (LOS) wireless communications by providing high spectral efficiency with a considerably low detection complexity. Similarly, index modulation (IM) schemes have been extensively studied over the past few years due to their attractive features, such as improved error performance, low complexity and high energy efficiency. In this paper, we propose the scheme of orbital angular momentum with index modulation (OAM-IM) by using the activated OAM modes themselves to carry additional information through the principle of IM. A general guideline is presented for the construction of optimal OAM-IM schemes along with the formulation of a low-complexity maximum likelihood (ML) detector. It is shown via computer simulations as well as theoretical bit error probability (BEP) calculations that the proposed OAM-IM schemes can achieve considerably better error performance than the reference OAM-MDM schemes while having a same level of detection complexity.**

***Index Terms*—Index modulation, line-of-sight wireless communications, MIMO systems, mode division multiplexing, orbital angular momentum.**

I. Introduction

RECENTLY announced key performance requirements of IMT-2020 have highlighted the significance of novel physical layer concepts to support lightning-speed and ultra-reliable communications for broadband systems and Internet of Things (IoT) applications of next-generation wireless networks [1]. Multiplexing in the form of multiple-input multiple-output (MIMO) transmission has been an integral part of the physical layer of modern wireless communication systems due to its attractive features, such as significantly improved overall throughput as well as high quality of service. In recent years, researchers have started to explore the potential of an alternative MIMO-based multiplexing scheme called *mode division multiplexing (MDM) using orbital angular momentum (OAM)*. According to electrodynamics, OAM is a physical characteristic of electromagnetic waves related with their field spatial distribution and can be used to create overlapping but orthogonal twisted beams, which can be exploited for communication purposes [2]. OAM is a relatively new wireless communication paradigm that is attracting more and more attention for potential short-distance line-of-sight (LOS) applications, such as high-bandwidth cellular backhaul communications and interconnections between computer clusters within a data center, which may have significant importance in 5G and beyond wireless networks. Apart from conventional radio frequency (RF) communications, OAM has been also explored extensively for free-space optical and fiber-optic communication systems [3], [4].

In order to create OAM-carrying fields, the authors of [5] considered uniform circular arrays (UCAs), in which equidistantly distributed antenna elements around the perimeter of a circle are phased with a $2\pi\ell/N$ phase difference from element to element, where N is the number of antenna elements in UCA and ℓ is the desired OAM mode number. The authors of [6] revealed that OAM communication system is a subset of traditional MIMO systems and does not provide additional capacity gains. On the other hand, recent studies have highlighted the attractive advantages of OAM-MDM systems, such as low-complexity transceiver design with completely eliminated inter-channel interference (ICI) and less stringent antenna synchronization. More specifically, OAM mode multiplexing/demultiplexing can be easily realized with phase shift networks that are passive RF devices; therefore, OAM-MDM schemes avoid additional post-processing overhead of traditional MIMO systems. In other words, while traditional MIMO systems rely on sophisticated digital signal processing for spatial multiplexing/demultiplexing, OAM schemes are capable of providing a much simpler implementation scenario.

A system model is introduced in [7] for the general multiple-mode OAM communication system composed of circular OAM generators arranged in concentric circles and the known properties of conventional MIMO systems are verified for OAM systems. In [8], unlike the previous OAM-MDM schemes that exploit different OAM modes to boost the spectral efficiency, the OAM topological charge (mode) number itself is used to carry information and the error probability of OAM mode detection is investigated. The authors of [9] analyzed the performance of the OAM scheme with computer simulations in the presence of system impairments such as antenna misalignment and receiver phase errors. The effective degrees of freedom of an OAM scheme is investigated with respect to the receiver circular array characteristics in [10]. The same authors of [7] and [10] focused on mode selection criteria in [11] and evaluated the capacity of various OAM mode combinations for the OAM multiplexing system. The study of [12] also investigated the capacity of the OAM system under different settings and showed that with perfect alignment, it is equivalent to that of traditional MIMO system. The RF link budget of a system employing OAM waves is studied in [13] with respect to the OAM topological charge and an asymptotic far-field formulation is developed for UCA-based OAM systems. The authors of [14] analyzed beam axis detection and alignment issues for UCA-based OAM systems employing a single OAM mode, and proposed three beam direction alignment schemes.

Manuscript received July 28, 2017; revised November 12, 2017; accepted December 26, 2017. Date of publication XXXX XX, 2017; date of current version XXXX XX, 2018. This work is supported in part by the Turkish Academy of Sciences Outstanding Young Scientist Award Programme (TUBA-GEBIP). The associate editor coordinating the review of this paper and approving it for publication was M. Di Renzo.

The author is with Istanbul Technical University, Faculty of Electrical and Electronics Engineering, 34469, Maslak, Istanbul, Turkey (e-mail: basarer@itu.edu.tr).

Color versions of one or more of the figures in this paper are available online at http://ieeexplore.ieee.org.

Digital Object Identifier 10.1109/TWC.2017.XXXXXXX

Promising new results and advancements on OAM-based radio communications have been reported within the past year. In [15], a new scheme utilizing both OAM and spin angular momentum, which is the well-known form of angular momentum, is proposed to enhance the system capacity through polarization. The authors of [16] proposed a novel OAM scheme with a partial arc sampling receiver (PASR) for compact receiving, i.e., to reduce the size of the receiver. A general signal model is presented and this scheme is experimentally realized in the presence of inter-mode crosstalk. Non-ideal receiver conditions, such as radial and angular deviation, are investigated through computer simulations for the OAM with PASR scheme in [17]. The same authors of [16] conducted a promising new experiment in [18] by realizing a four-mode OAM-MDM scheme operating at the microwave frequency of 10 GHz to quadruple the spectral efficiency. This work also highlighted the attractive features of OAM-based schemes, such as high spectral efficiency and considerably low receiver complexity, compared to traditional MIMO solutions. Another inspiring experiment is recently performed by the authors of [19], in which the combination of OAM-MDM and a conventional 2×2 spatial multiplexing system is explored to provide design flexibility and increase the overall capacity. A millimeter-wave communication system, operating at 26 GHz and employing two-mode OAM-MDM, is constructed to transmit data at a rate of 16 Gbps over a short distance of 1.8 meters. In [20], an OAM-based full-duplex communication system is designed for bidirectional communications and the sum-rate of the system is maximized through the optimal OAM mode pair. Finally, trellis coded union modulation of quadrature amplitude modulation (QAM) and OAM is considered in [21] by exploiting OAM as a new dimension in the signal constellation.

Index modulation (IM) is a novel digital modulation concept that utilizes the indices of the building blocks of the corresponding communication systems in an on/off keying fashion to transmit additional information bits. IM also appears as a promising technology for 5G and beyond wireless networks [22]. Three most noticeable forms of IM is spatial modulation (SM) [23], orthogonal frequency division multiplexing (OFDM) with IM [24] and channel modulation (CM) [25] schemes, which consider the indices of the available transmit antennas, OFDM subcarriers and RF mirrors mounted at a reconfigurable antenna, respectively. Recently, the family of single-carrier based IM has been extended to massive MIMO systems [26], and link adaptive designs and multi-user applications have been investigated. The application of SM to millimeter-wave communications is investigated in [27]. Power allocation [28] and transmit precoding [29] issues are explored for SM to improve its performance. The promising potential of IM has also been explored for optical wireless communications [30]–[32], spread spectrum systems [33] and non-orthogonal waveforms [34], [35]. Within this perspective, the available orthogonal modes of OAM provide an interesting new direction for the application of IM.

In this paper, we propose the scheme of *orbital angular momentum with index modulation (OAM-IM)* by utilizing the active OAM modes themselves to convey information. In other words, our aim is to explore the promising potential of IM in the emerging field of OAM by transmitting information by not only traditional data symbols as in OAM-MDM systems but also by the active mode combinations of OAM in an attempt to further improve the error performance through IM. Our novel contributions are summarized as follows:

- We introduce the concept of OAM-IM by activating a subset of the available OAM modes to carry information.
- We derive the theoretical bit error probability (BEP) of the OAM-IM scheme and then optimize the signal constellations employed by different active OAM mode combinations to achieve the optimal bit error rate (BER) performance. We also provide a general guideline for the design of OAM-IM schemes with different configurations.
- We develop a log-likelihood ratio (LLR) calculation based low-complexity maximum likelihood (ML) detector for OAM-IM, which has the same order of detection complexity as that of OAM-MDM.
- By extensive computer simulations, we prove the superiority of the proposed OAM-IM scheme compared to traditional OAM-MDM for both perfect and imperfect orthogonality of OAM modes.

The rest of the paper is organized as follows. In Section II, we introduce the system model of the proposed scheme. Section III deals with the performance analysis and optimization of OAM-IM. We propose a low-complexity ML detector for OAM-IM in Section IV. Computer simulation results are given in Section V and Section VI concludes the paper[1].

II. System Model

We consider two aligned UCAs facing each other and consisting of N elements for the transmission and reception of OAM signals as seen from Fig. 1. The distance between the centers of UCAs is d and the radii of transmit and receive UCAs are given by r_{tx} and r_{rx}, respectively. For this case, the total number of possible OAM modes that can be generated becomes N [13], while the number of activated modes is denoted by N_A for the OAM-IM scheme, where $N_A \in \{1, 2, \ldots, N\}$. Here, we apply the on/off keying mechanism of IM [36] to activate only a subset of the available OAM modes, similar to the transmit antennas of SM and subcarriers of OFDM-IM, to convey information in an energy-efficient way. Since we map information bits to the indices of active OAM modes and each activated mode conveys an M-ary phase shift keying (PSK) or QAM symbol, the spectral efficiency (in terms of bits per channel use (bpcu)) of the OAM-IM scheme is obtained as

$$\eta = N_A \log_2 M + \left\lfloor \log_2 \binom{N}{N_A} \right\rfloor. \tag{1}$$

[1]*Notation*: Bold, lowercase and capital letters are used for column vectors and matrices, respectively. $(\cdot)^{\text{T}}$ and $(\cdot)^{\text{H}}$ denote transposition and Hermitian transposition, respectively. $\|\cdot\|$ stands for the Euclidean norm. $\binom{\cdot}{\cdot}$, $\lfloor\cdot\rfloor$ and $\lceil\cdot\rceil$ denote the binomial coefficient, floor and ceil functions, respectively. $\text{eig}(\cdot)$ returns the eigenvalues of a matrix as a vector, while $\text{diag}(\cdot)$ forms a diagonal matrix from a vector. $\mathbf{I}_N$ is the identity matrix with dimensions $N \times N$. The probability of an event is denoted by $P(\cdot)$ and $E\{\cdot\}$ stands for expectation. $Q(\cdot)$ is the Gaussian Q-function. $\mathcal{S}$ represents the M-ary signal constellation.

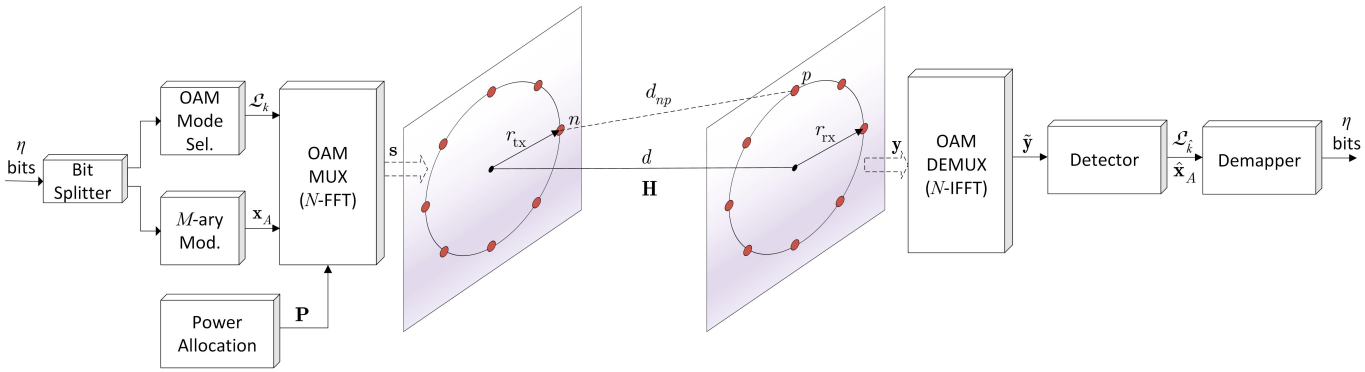

Fig. 1. Block diagram of the OAM-IM transceiver.

It should be noted that OAM-MDM becomes the special case of OAM-IM for $N_A = N$, i.e., when all modes are activated, while for $N_A = 1$, an SM type OAM scheme, which activates a single OAM mode, is obtained. We also note that a similar type of OAM scheme, which generates a single OAM mode among the set of possible OAM modes for data transmission, is reported in [8]. However, this scheme is more analogous to space shift keying (SSK) [23] since it does not consider ordinary M-ary modulation.

To radiate an OAM wave with mode number ℓ, the same input signal (x_ℓ) should be applied to the antenna elements in UCA with a successive phase shift from element to element. Consequently, the signal applied to the nth element is given for $n = 0, 1, \ldots, N-1$ as

$$s_n^\ell = \frac{1}{\sqrt{N}} p_\ell x_\ell e^{-j2\pi \frac{n\ell}{N}} \tag{2}$$

where p_ℓ is the power allocation factor of mode ℓ. With MDM principle of OAM, the antenna element $n \in \{0, 1, \ldots, N-1\}$ is fed by the linear superposition of the signals of different modes as

$$s_n = \sum_{\ell \in \mathcal{L}_k} s_n^\ell = \frac{1}{\sqrt{N}} \sum_{\ell \in \mathcal{L}_k} p_\ell x_\ell e^{-j2\pi \frac{n\ell}{N}} \tag{3}$$

where $\mathcal{L}_k = \{k_1, k_2, \ldots, k_{N_A}\}$ is the set of activated OAM modes for the kth active mode combination of OAM-IM, where $k \in \{1, 2, \ldots, n_c\}$ and $n_c = 2^{\left\lfloor \log_2 \binom{N}{N_A} \right\rfloor}$ is the total number of different active mode combinations. Please note that while $\mathcal{L}_1 = \{0, 1, \ldots, N-1\}$ for classical OAM-MDM, the set of activated OAM-IM modes is determined according to the information bits in each signaling interval. It should be also noted that due to alising (discrete sampling), the OAM modes with $\ell > N/2$ correspond to the modes with negative orders as $\ell - N$. Considering (3), the transmission vector of the proposed scheme can be expressed as

$$\mathbf{s} = \mathbf{W}\mathbf{P}\mathbf{x} \tag{4}$$

where $\mathbf{P} = \text{diag}\left(\begin{bmatrix} p_0 & p_1 & \cdots & p_{N-1} \end{bmatrix}\right)$ is the power allocation matrix, which ensures that the received signal-to-noise ratio (SNR) is the same for all possible activated OAM modes under the (average) total transmission power constraint of $P_t = \sum_{\ell=0}^{N-1} p_\ell^2$, $\mathbf{W} \in \mathbb{C}^{N \times N}$ is the discrete Fourier transform (DFT) matrix and $\mathbf{x} = \begin{bmatrix} x_0 & x_1 & \cdots & x_{N-1} \end{bmatrix}^{\text{T}}$ is the vector of complex data symbols that contains some zero terms due to IM, whose positions carry additional information. More specifically, the non-zero entries of $\mathbf{x}$, whose indices are in the set of $\mathcal{L}_k$, contain a total of N_A complex data symbols $(d_{k_1}, d_{k_2}, \ldots, d_{k_{N_A}})$ that are obtained at the output of M-ary modulator in the form of $\mathbf{x}_A \in \mathbb{C}^{N_A \times 1}$. In order to have the same total transmission power as that of OAM-MDM, i.e., for $E\left\{\mathbf{x}^{\text{H}}\mathbf{x}\right\} = N$, which is equivalent to $E\left\{\mathbf{s}^{\text{H}}\mathbf{s}\right\} = P_t$ under the assumption of equiprobable OAM mode activation, the non-zero elements of $\mathbf{x}$ are amplified as

$$\mathbf{x} = \alpha \begin{bmatrix} 0 & \cdots & d_{k_1} & 0 & \cdots & d_{k_{N_A}} & \cdots & 0 \end{bmatrix}^{\text{T}} \tag{5}$$

where $\alpha = \sqrt{N/N_A}$ is an amplification factor used to transfer the saved energy from the inactive modes to the active ones due to IM. It should be noted that due to activation of different modes in each signaling interval, even if a constant envelope modulation such as binary/quadrature PSK (BPSK/QPSK) is used, the total transmission power of the OAM-IM scheme is not constant at all times, while its average is P_t.

The complex baseband signal model of the OAM-IM scheme is given as

$$\mathbf{y} = \mathbf{H}\mathbf{s} + \mathbf{n} \tag{6}$$

where $\mathbf{y} \in \mathbb{C}^{N \times 1}$ is the vector of received signals, $\mathbf{H} \in \mathbb{C}^{N \times N}$ is the channel matrix that characterizes the LOS propagation environment and $\mathbf{n} \in \mathbb{C}^{N \times 1}$ is the vector of additive white Gaussian noise samples with variance σ_n^2. The free-space channel response between nth transmitter and pth receiver elements is calculated by

$$h_{pn} = \beta \frac{\lambda}{4\pi d_{np}} e^{-jkd_{np}} \tag{7}$$

where $k = 2\pi/\lambda$ with λ being the wavelength, β is a constant related with antenna gains and d_{np} is the distance between the antenna elements, which is given by the following for the case of perfect alignment between transmit and receive UCAs:

$$d_{np} = \sqrt{d^2 + r_{\text{tx}}^2 + r_{\text{rx}}^2 - 2r_{\text{tx}}r_{\text{rx}}\cos\phi_{np}} \tag{8}$$

where $\phi_{np} = \frac{2\pi(n-p)}{N}$. It should be noted that due to the employment of UCAs at both transmitter and receiver sides as well as the construction of a configuration with perfect symmetry, $\mathbf{H}$ becomes a circulant matrix.

At the receiver, the receive phase-shift network recovers the signals transmitted with different OAM modes as

$$\tilde{y}_\ell = \frac{1}{\sqrt{N}} \sum_{p=0}^{N-1} y_p e^{j2\pi \frac{p\ell}{N}} \tag{9}$$

for $\ell = 0, 1, \ldots, N-1$, where y_p is the pth element of $\mathbf{y}$. The above OAM mode demultiplexing can be realized by the processing of the vector of received signals $\mathbf{y}$ with the inverse DFT (IDFT) matrix $\mathbf{W}^{\mathrm{H}}$ as

$$\begin{aligned} \mathbf{W}^{\mathrm{H}}\mathbf{y} &= \mathbf{W}^{\mathrm{H}}\mathbf{H}\mathbf{s} + \mathbf{W}^{\mathrm{H}}\mathbf{n} \\ \tilde{\mathbf{y}} &= \mathbf{W}^{\mathrm{H}}\mathbf{H}\mathbf{W}\mathbf{P}\mathbf{x} + \tilde{\mathbf{n}} \\ &= \mathbf{\Lambda}\mathbf{P}\mathbf{x} + \tilde{\mathbf{n}} \end{aligned} \tag{10}$$

where $\mathbf{\Lambda} \in \mathbb{C}^{N\times N}$ is a diagonal matrix that is obtained by the diagonalization of the circulant channel matrix $\mathbf{H}$ by the DFT matrix and contains the eigenvalues of $\mathbf{H}$ $(\xi_0, \xi_1, \ldots, \xi_{N-1})$, i.e.,

$$\mathbf{\Lambda} = \mathrm{diag}(\mathrm{eig}\,(\mathbf{H})) = \sqrt{N}\mathrm{diag}\,(\mathbf{W}\mathbf{h}_1) \tag{11}$$

where $\mathbf{h}_1$ is the first column of $\mathbf{H}$. Power allocation ensures that all OAM modes have the same received SNR, that is, the absolute values of the diagonal elements of $\mathbf{G}$ are the same, where $\mathbf{G} = \mathbf{\Lambda}\mathbf{P}$. To satisfy this, the power allocation factor of mode ℓ is determined as

$$p_\ell = \sqrt{\frac{\frac{P_t}{|\xi_\ell|^2}}{\frac{1}{|\xi_0|^2} + \frac{1}{|\xi_1|^2} + \cdots + \frac{1}{|\xi_{N-1}|^2}}}. \tag{12}$$

In other words, the power allocation factor of each mode is inversely proportional with the corresponding eigenvalue of the circulant channel matrix, while the activated modes share the total transmission power of P_t in average.

We define the SNR as $\frac{P_t/\eta}{\sigma_n^2}$, which is equivalent to E_b/N_0, where E_b is the average transmitted energy per bit and N_0 is the noise power spectral density.

In Section III, we provide a guideline for the construction of optimal OAM-IM schemes with varying system parameters.

A. ML Detection of OAM-IM

The input-output relationship of the OAM-IM scheme can be rewritten from (10) as

$$\tilde{\mathbf{y}} = \mathbf{G}\mathbf{x} + \tilde{\mathbf{n}}. \tag{13}$$

Since $\mathbf{G}$ is a diagonal matrix, different OAM modes do not interfere with each other and each substream can be detected individually for the OAM-MDM system. However, due to the index information carried by active OAM modes in OAM-IM, its ML detector has to make a joint search over all possible realizations of active modes and complex data symbols as

$$(\hat{k}_1, \ldots, \hat{k}_{N_A}, \hat{d}_{\hat{k}_1}, \ldots, \hat{d}_{\hat{k}_{N_A}}) = \arg \min_{\mathcal{L}_k, \mathbf{x}_A} \|\tilde{\mathbf{y}} - \mathbf{G}\mathbf{x}\|^2. \tag{14}$$

This detector requires $(4N_A + 2N)n_c M^{N_A}$ real multiplications (RMs) and $(4N_A + 2N - 1)n_c M^{N_A}$ real additions (RAs), which correspond to a detection complexity order of $\sim \mathcal{O}(n_c N M^{N_A})$ in terms of real operations. Since the complexity of the ML detector grows exponentially with N_A, it may put too much stress on the receiver hardware with increasing spectral efficiency values. In Section IV, we propose a low-complexity ML detector based on LLR calculation.

III. Performance Analysis and Optimization of OAM-IM

In this section, we first derive the theoretical BEP of the OAM-IM scheme and then optimize the signal constellations employed by the activated OAM modes to improve the overall error performance.

Based on the signal model of (13) and ML detection, the pairwise error probability (PEP) for the detection of $\hat{\mathbf{x}}$ instead of $\mathbf{x}$ can be expressed as

$$\begin{aligned} P(\mathbf{x} \to \hat{\mathbf{x}}) &= P\left(\|\tilde{\mathbf{y}} - \mathbf{G}\mathbf{x}\|^2 > \|\tilde{\mathbf{y}} - \mathbf{G}\hat{\mathbf{x}}\|^2\right) \\ &= Q\left(\sqrt{\frac{\Delta}{2\sigma_n^2}}\right) \approx \frac{1}{12}e^{-\Delta/(4\sigma_n^2)} + \frac{1}{4}e^{-\Delta/(3\sigma_n^2)} \end{aligned} \tag{15}$$

where $\Delta = \|\mathbf{G}(\mathbf{x} - \hat{\mathbf{x}})\|^2$. Since we consider a non-fading scenario, the PEP of (15) can be easily calculated for a given pair of $\mathbf{x}$ and $\hat{\mathbf{x}}$, while a tight upper bound on BEP is calculated from

$$P_b \approx \frac{1}{2^\eta} \sum_{\mathbf{x}} \sum_{\hat{\mathbf{x}}} \frac{P(\mathbf{x} \to \hat{\mathbf{x}})\, e(\mathbf{x}, \hat{\mathbf{x}})}{\eta} \tag{16}$$

where $e(\mathbf{x}, \hat{\mathbf{x}})$ stands for the number of bit errors for the corresponding error event. As seen from (15), the PEP is directly dependent on the squared Euclidean distances between different OAM-IM transmission vectors since $\mathbf{G}^{\mathrm{H}}\mathbf{G} = G\mathbf{I}_N$. To improve the overall PEP performance, we introduce rotation to the signal constellations employed by different active OAM mode combinations to maximize the minimum squared Euclidean distance that is defined as $d_{\min} = \min_{\mathbf{x},\hat{\mathbf{x}}} \|\mathbf{x} - \hat{\mathbf{x}}\|^2$. We also consider $d_{\min}$ to evaluate the error performance of the system with and without constellation rotation. We apply the following procedures for the design of the optimal OAM-IM scheme (in terms of maximum $d_{\min}$) for given system parameters of N, N_A and M:

1) Calculate the total number of active OAM mode combinations from $n_c = 2^{\left\lfloor \log_2 \binom{N}{N_A} \right\rfloor}$.
2) Since $d_{\min}$ is highly dependent to the combinations with common active OAM modes, divide the whole set of combinations into distinct subsets composed of combinations with non-overlapping active modes. The maximum number of non-overlapping combinations in each subset is $n_d = \lfloor N/N_A \rfloor$, while the number of subsets is $n_s = \lceil n_c/n_d \rceil$.
3) Assign a different rotation angle θ_i for each subset i, where $\theta_1 = 0$ and $\theta_i = \frac{2(i-1)\pi}{M n_s}, i \in \{2, 3, \ldots, n_s\}$ for M-PSK. The optimum angles can be found with an exhaustive search for M-QAM constellations.

The logic behind this design (partitioning and constellation rotation) is explained as follows. Considering the effects of

TABLE I
PARAMETERS OF THE DESIGNED OAM-IM SCHEMES

N	N_A	M	n_c	n_d	n_s	$d_{\min}^{\mathcal{S}}$	$d_{\min}^{\text{OAM}}$	$d_{\min}$	η	$\{\theta_i\}_{i=2}^{n_s}$	Active Mode Combinations $\{\mathcal{L}_k\}_{k=1}^{n_c}$
4	1	2	4	4	1	16	8	8	3	-	$\{(0),(1),(2),(3)\}$
4	2	2	4	2	2	8	8	8	4	$\{\pi/2\}$	$\{(0,1),(2,3),(0,2),(1,3)\}$
4	2	4	4	2	2	4	5.172	4	6	$\{\pi/4\}$	
4	2	16	4	2	2	0.8	0.878	0.8	10	$\{0.445\}$	
4	2	64	4	2	2	0.190	0.196	0.190	14	$\{0.236\}$	
4	3	2	4	1	4	5.333	4.229	4.229	5	$\{\pi/4,\pi/2,3\pi/4\}$	$\{(0,1,2),(0,1,3),(0,2,3),(1,2,3)\}$
4	3	4	4	1	4	2.667	3.073	2.667	8	$\{\pi/8,\pi/4,3\pi/8\}$	
4	3	8	4	1	4	0.889	0.978	0.889	11	$\{\pi/8,\pi/4,3\pi/8\}$	
6	2	2	8	3	3	12	9	9	5	$\{\pi/3,2\pi/3\}$	$\{(0,1),(2,3),(4,5),(0,5),(1,2),(3,4),(0,2),(1,3)\}$
6	2	4	8	3	3	6	6.804	6	7	$\{\pi/6,\pi/3\}$	
8	2	2	16	4	4	16	10.343	10.343	6	$\{\pi/4,\pi/2,3\pi/4\}$	$\{(0,1),(2,3),(4,5),(6,7),(0,7),(1,2),(3,4),(5,6),$
8	2	4	16	4	4	8	8.609	8	8	$\{\pi/8,\pi/4,3\pi/8\}$	$(0,2),(1,3),(4,6),(5,7),(0,4),(1,5),(2,6),(3,7)\}$

active OAM mode errors and M-ary symbol errors separately, $d_{\min}$ can be also calculated via

$$d_{\min} = \min\left\{d_{\min}^{\mathcal{S}}, d_{\min}^{\text{OAM}}\right\} \tag{17}$$

where $d_{\min}^{\mathcal{S}}$ is the minimum squared Euclidean distance corresponding to the correct detection of all activated OAM modes and the erroneous detection of a single data symbol. On the other hand, $d_{\min}^{\text{OAM}}$ is the minimum squared Euclidean distance corresponding to the worst case error event due to mode detection errors. Without loss of generality, for the case of $n_s = 2$, we can consider the following two generic pairs for a deeper investigation of (17): $\mathbf{x} = \alpha\left[d_0 \;\; d_1 \;\; 0 \;\; 0\right]^{\text{T}}$, $\hat{\mathbf{x}} = \alpha\left[\hat{d}_0 \;\; \hat{d}_1 \;\; 0 \;\; 0\right]^{\text{T}}$ and $\mathbf{x} = \alpha\left[d_0 \;\; d_1 \;\; 0 \;\; 0\right]^{\text{T}}$, $\hat{\mathbf{x}} = \alpha e^{j\theta_2}\left[\hat{d}_0 \;\; 0 \;\; \hat{d}_2 \;\; 0\right]^{\text{T}}$, where $N = 4$ and $N_A = 2$. Considering the first pair, in which no mode detection errors occur, we observe that $d_{\min}^{\mathcal{S}} = \alpha^2 d_{\min}^{\text{PSK(QAM)}}$, where $d_{\min}^{\text{PSK(QAM)}}$ is the minimum squared Euclidean distance of the considered PSK (QAM) constellation, i.e., $d_{\min}^{\text{PSK}} = 4\sin^2(\pi/M)$ and $d_{\min}^{\text{QAM}} = 6/(M-1)$. From the second pair, we have

$$\begin{aligned} d_{\min}^{\text{OAM}} &= \min_{d_0,\hat{d}_0,d_1,\hat{d}_2} \alpha^2\left(\left|d_1\right|^2 + \left|\hat{d}_2\right|^2 + \left|d_0 - \hat{d}_0 e^{j\theta_2}\right|^2\right) \\ &= \min_{d_0,\hat{d}_0} \alpha^2\left(2E_{s,\min} + \left|d_0 - \hat{d}_0 e^{j\theta_2}\right|^2\right) \end{aligned} \tag{18}$$

where $E_{s,\min}$ is the energy of the constellation symbol with the minimum energy, i.e., $E_{s,\min} = 1$ for M-PSK and $E_{s,\min} = 3/(M-1)$ for square M-QAM. To reduce the probability of OAM mode detection errors as well as to increase $d_{\min}$, $d_{\min}^{\text{OAM}}$ should be maximized. It should be noted that without constellation rotation ($\theta_2 = 0$), the term of $\left|d_0 - \hat{d}_0 e^{j\theta_2}\right|^2$ in (18) vanishes for $d_0 = \hat{d}_0$, which reduces $d_{\min}^{\text{OAM}}$ to $2\alpha^2 E_{s,\min}$. For M-PSK, it can be easily verified that by selecting the corresponding rotation angle θ_2 according to the symmetry, i.e., $\theta_2 = \pi/M$, $d_{\min}^{\text{OAM}}$ can be maximized. On the other hand, the optimum value of θ_2 must be found through a computer search for M-QAM. In Fig. 2, we plot $d_{\min}^{\text{OAM}}$ as a function of θ_2 for different constellations. From Fig. 2, we obtain the optimum θ_2 for 16-QAM and 64-QAM as 0.445 rad and 0.236 rad, respectively.

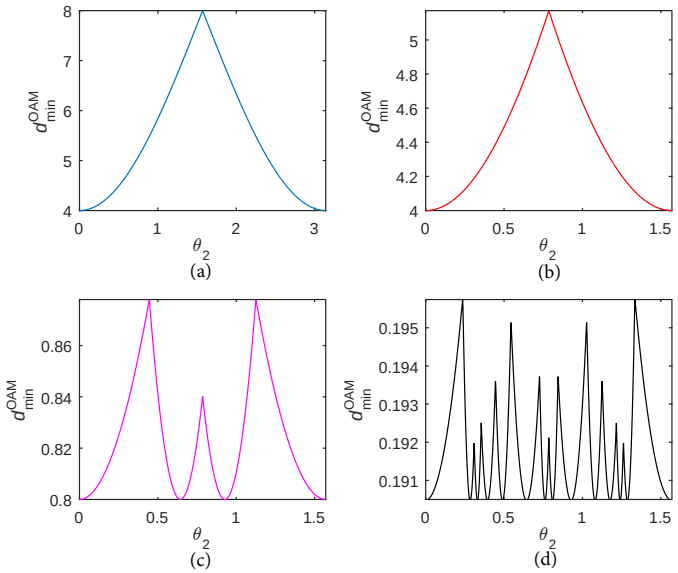

Fig. 2. Variation of $d_{\min}^{\text{OAM}}$ with θ_2 for (a) BPSK, (b) QPSK, (c) 16-QAM and (d) 64-QAM ($n_s = 2, \alpha = 2$).

For the general case of $n_s > 2$, due to the symmetry, the optimal rotation angles for M-PSK can be given as $\theta_i = \frac{2(i-1)\pi}{M n_s}$ for $i = 1, 2, \ldots, n_s$ since this selection ensures a uniform minimum distance between different subsets of active mode combinations. On the other hand, the determination of the optimum rotation angles for the case of M-QAM requires an exhaustive search. However, the selection of the same rotation angles as that of M-PSK can provide a satisfactory performance. It is also important to note that the optimization of rotation angles is more critical for smaller constellations, such as BPSK and QPSK as also seen from Fig. 2, while $d_{\min}^{\mathcal{S}}$ dictates the overall $d_{\min}$ for higher order constellations.

In Table I, we list the main parameters of the considered OAM-IM schemes that are designed according to the procedures given in this section. From the perspective of a system designer, for a specific configuration and target bpcu, the emphasis should be given to the systems with higher $d_{\min}$ to obtain the optimal BER performance.

IV. Low Complexity ML Detection of OAM-IM

In this section, we develop a low-complexity ML detector based on LLR calculation for the OAM-IM scheme. This detector is inspired from the LLR detector of OFDM-IM [24] and calculates a probabilistic measure regarding the active status of each OAM mode considering the demultiplexed received signals.

Let us rewrite (13) in scalar form as

$$\tilde{y}_\ell = g_\ell x_\ell + \tilde{n}_\ell, \quad \ell = 0, 1, \ldots, N-1 \tag{19}$$

where the four terms in (19) stand for the corresponding elements of $\tilde{\mathbf{y}}$, $\mathbf{G}$, $\mathbf{x}$ and $\tilde{\mathbf{n}}$, respectively. In order to assess the active status of each mode ℓ, the LLR detector of the OAM-IM scheme calculates the following n_s LLR values considering that the target mode can be inactive ($x_\ell = 0$) or active (carrying an M-ary symbol from the constellation $\alpha\mathcal{S}e^{j\theta_i}$, where $i \in \{1, 2, \ldots, n_s\}$ and $\alpha = \sqrt{N/N_A}$):

$$\begin{aligned}\lambda_\ell^i &= \ln \frac{\sum_{d\in\mathcal{S}e^{j\theta_i}} P\left(x_\ell = \alpha d \mid \tilde{y}_\ell\right)}{P\left(x_\ell = 0 \mid \tilde{y}_\ell\right)} \\ &= c + \frac{|\tilde{y}_\ell|^2}{\sigma_n^2} + \ln\left(\sum_{d\in\mathcal{S}e^{j\theta_i}} \exp\left(-\frac{1}{\sigma_n^2}\left|\tilde{y}_\ell - g_\ell \alpha d\right|^2\right)\right)\end{aligned} \tag{20}$$

where c stands for the constant terms and can be ignored. Then, the LLR detector calculates LLR sums for each active mode combination $k \in \{1, 2, \ldots, n_c\}$ as

$$\lambda^k = \sum\nolimits_{\ell\in\mathcal{L}_k} \lambda_\ell^{\lceil k/n_d \rceil} \tag{21}$$

where $\mathcal{L}_k$ was defined in (3). At the last step, the most likely active mode combination is determined from

$$\hat{k} = \arg\max_k \lambda^k. \tag{22}$$

Once the combination of active modes is determined, the corresponding data symbols can be recovered independently from each other by

$$\hat{d}_\ell = \arg\min_{d\in\mathcal{S}e^{j\psi}} \left|\tilde{y}_\ell - g_\ell \alpha d\right|^2 \tag{23}$$

for $\ell \in \mathcal{L}_{\hat{k}}$, where $\psi = \theta_{\lceil \hat{k}/n_d \rceil}$. Finally, the demapper provides an estimate of the input bit stream from the detected active mode combination and data symbols. As seen from (20)-(23), the LLR detector requires $7NMn_s + 3N$ RMs and $6NMn_s + n_c(N_A - 1) + N$ RAs, which correspond to a detection complexity order of $\sim \mathcal{O}(NMn_s)$ in terms of real operations. This value is significantly lower than that of the ML detector $\left(\sim \mathcal{O}(n_c N M^{N_A})\right)$. In other words, LLR calculation based detector of the OAM-IM scheme provides a linear detection complexity by cleverly decoupling the joint detection problem of the active modes and data symbols. Since this detector considers all possible legitimate active mode combinations, it also provides an ML solution, which will be verified in Section V. It is also important to note that the ML detection complexity order of the OAM-MDM scheme is $\sim\mathcal{O}(NM)$, which is slightly lower than that of OAM-IM, since its ML detector requires $6NM$ RMs and $5NM$ RAs.

In the following, we provide an example for the operation of the proposed low-complexity ML detector.

TABLE II
Simulation Parameters

Operation frequency (f_c)	10 GHz
Wavelength (λ)	0.03 m
Tx UCA radius (r_{tx})	0.6 m
Rx UCA radius (r_{rx})	0.6 m
UCA configurations	$4\times4, 6\times6, 8\times8$
Transmission distance (d)	500λ m
Average transmission power (P_t)	1 W
Antenna parameter (β)	1

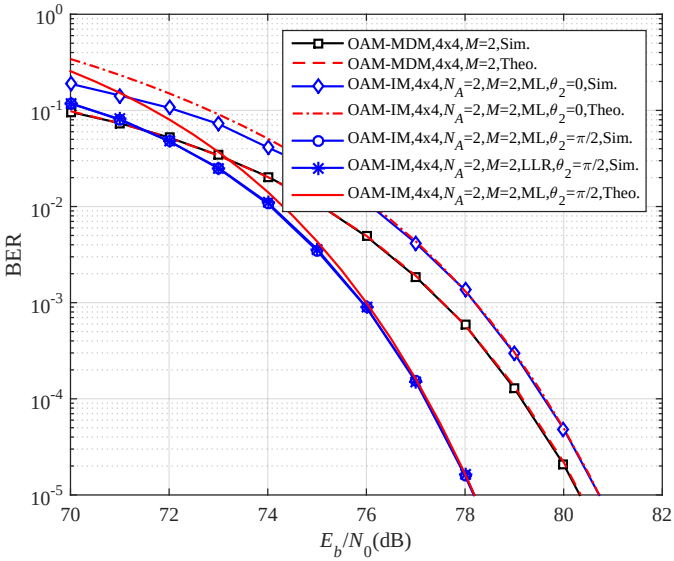

Fig. 3. OAM-IM and OAM-MDM comparison with different type of detectors and with/without constellation rotation (4×4 configuration, $M = 2, \eta = 4$).

Example: Let us consider the OAM-IM scheme with $N = 4$ and $K = 2$ parameters. From Table I, we have $n_c = 4$ combinations: $\mathcal{L}_1 = (0, 1)$, $\mathcal{L}_2 = (2, 3)$, $\mathcal{L}_3 = (0, 2)$ and $\mathcal{L}_4 = (1, 3)$, which are grouped in $n_s = 2$ subsets each containing $n_d = 2$ non-overlapping combinations. Considering $\mathcal{S}$ and $\mathcal{S}e^{j\theta_2}$ constellations, the LLR detector calculates the following eight LLR values from (20): $\lambda_0^1, \lambda_1^1, \lambda_2^1, \lambda_3^1$ and $\lambda_0^2, \lambda_1^2, \lambda_2^2, \lambda_3^2$. Then, the following four LLR sums are obtained respectively for four possible combinations using (21):

$$\begin{aligned}\lambda^1 &= \lambda_0^1 + \lambda_1^1, \qquad \lambda^2 = \lambda_2^1 + \lambda_3^1, \\ \lambda^3 &= \lambda_0^2 + \lambda_2^2, \qquad \lambda^4 = \lambda_1^2 + \lambda_3^2.\end{aligned} \tag{24}$$

At the last step, the most likely combination is determined by $\hat{k} = \arg\max_k \lambda^k$, where $k \in \{1, 2, 3, 4\}$. Considering that $\psi = 0$ and $\psi = \theta_2$ for $\hat{k} \in \{1, 2\}$ and $\hat{k} \in \{3, 4\}$, respectively, the corresponding data symbols conveyed by the active modes with indices $\mathcal{L}_{\hat{k}}$ are recovered from (23). □

V. Simulation Results

In this section, we evaluate the bit error rate (BER) performance of the proposed OAM-IM scheme and make comparisons with the OAM-MDM scheme. Our computer simulation parameters are shown in Table II.

This article has been accepted for publication in a future issue of this journal, but has not been fully edited. Content may change prior to final publication. Citation information: DOI 10.1109/TWC.2017.2787992, IEEE Transactions on Wireless Communications

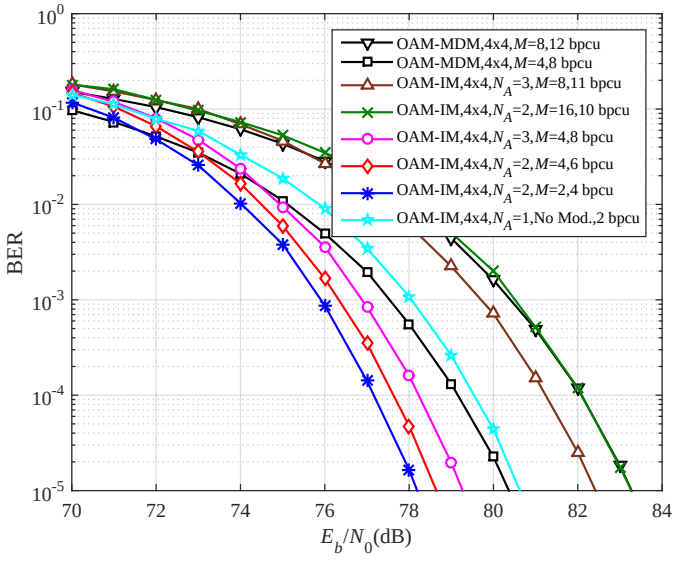

Fig. 4. OAM-IM and OAM-MDM comparison for different spectral efficiency values (4×4 configuration).

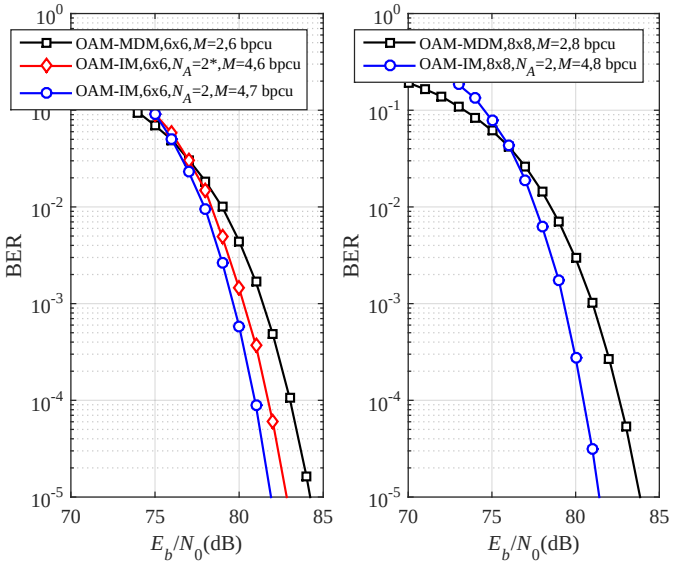

Fig. 5. OAM-IM and OAM-MDM comparison for (a) 6×6 (b) 8×8 configurations.

In Fig. 3, we compare the BER performance of the OAM-IM scheme with OAM-MDM for a 4×4 configuration and BPSK. Several important remarks can be inferred from Fig. 3. First, the derived theoretical BEP upper bounds are considerably accurate for increasing SNR values. Please note that the theoretical BEP of OAM-MDM can be easily obtained for BPSK (or QPSK) as $P_b = Q\left(\sqrt{2GNE_b/N_0}\right)$, where the factors G and N come from the LOS channel and the definition of SNR (we have $E_b = 1/\eta$ under unity symbol duration assumption), respectively. Since the received SNR is directly determined by G, which is obtained from $\mathbf{G}^{\mathrm{H}}\mathbf{G} = G\mathbf{I}_N$ as $G = 2.087 \times 10^{-8}$ for this configuration, the provided BER curves are approximately 75 dB adrift from the case of traditional AWGN transmission. Second, while the OAM-IM scheme provides a worse BER performance than the OAM-MDM scheme for $\theta_2 = 0$, it provides a significant improvement for $\theta_2 = \pi/2$, which increases the overall $d_{\min}$ from 4 to 8. Since $d_{\min} = 4$ for the OAM-MDM scheme, a 3 dB coding gain is asymptotically expected from the OAM-IM scheme, which is in accordance with our BER results. Third, we observe that LLR and brute-force ML detectors exhibit the same error performance, which is an expected result, considering the optimal nature of the LLR detector.

In Fig. 4, we consider the operation of the 4×4 OAM-IM scheme with different spectral efficiency values. We observe that for 8 bpcu transmission, OAM-IM scheme with $N_A = 3$ and $M = 4$ provides a better BER performance than the reference OAM-MDM scheme with $M = 4$. This improvement can be explained by the OAM-IM scheme's asymptotic coding gain of $10\log_{10}(2.667/2) = 1.25$ dB over the reference OAM-MDM scheme. It is important to note that by reducing the spectral efficiency, an even better BER performance can be obtained by the OAM-IM scheme with 4 and 6 bpcu transmissions. As a result, we conclude that OAM-IM provides an interesting trade-off between error performance and spectral efficiency. However, the OAM-IM scheme with $N_A = 1$ and no M-ary modulation, which is equivalent to the scheme of [8], suffers from a worse BER performance compared to the OAM-IM scheme with $N_A = 2$ and $M = 2$ due to its lower η value. Finally, it is revealed that while the OAM-IM scheme with $N_A = 2$ and $M = 16$ provides a very close BER performance to the reference OAM-MDM scheme with $M = 8$, the OAM-IM scheme with $N_A = 3$ and $M = 8$ exhibits a more satisfactory performance due to its higher $d_{\min}$. It is worth noting that plain IM schemes such as SM, SSK, OFDM-IM etc., generally suffer at high spectral efficiency due to the nature of the IM mechanism that leaves some of the available transmit resources empty for IM. Therefore, the improvements offered by the proposed OAM-IM scheme at higher spectral efficiency values look promising to unlock the potential of IM-based solutions.

We extend our computer simulations to 6×6 and 8×8 configurations in Fig. 5, and make comparisons with the reference OAM-MDM schemes. We observe from Fig. 5 that a better BER performance can be obtained in both cases. It is important to note that for the 6×6 case, a better BER performance is obtained even if a higher spectral efficiency is offered than the reference OAM-MDM scheme[2].

Finally, we conclude that the improvements provided by the OAM-IM schemes come at the price of a minor increase in detection complexity due to the employment of multiple signal constellations through constellation rotation. As we discussed in Section IV, we employ an LLR-based low-complexity ML detector for OAM-IM, which has a linearly increasing detection complexity (with respect to N and M) similar to the ML detector of OAM-MDM.

In Fig. 6, we consider the case of imperfect alignment

[2]To achieve 6 bpcu ($N_A = 2^*$ scheme), we consider only the first four combinations given in Table I for $N = 6, N_A = 2$ and $\theta_2 = \pi/4$. Since the modes are not activated with equal probability for 6×6 schemes, the corresponding amplification factors are adjusted as $\alpha = 1.652$ and $\alpha = 1.781$ for 6 and 7 bpcu schemes, respectively, to ensure unity transmission power.

This article has been accepted for publication in a future issue of this journal, but has not been fully edited. Content may change prior to final publication. Citation information: DOI 10.1109/TWC.2017.2787992, IEEE Transactions on Wireless Communications

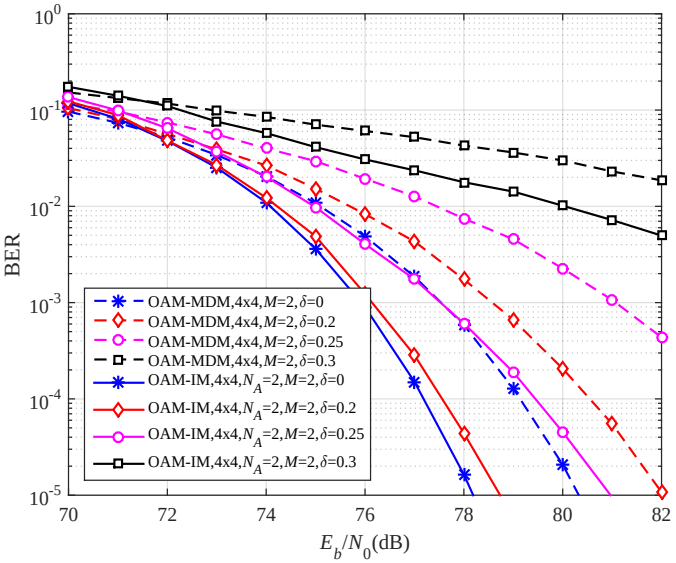

Fig. 6. OAM-IM and OAM-MDM comparison for imperfect alignment.

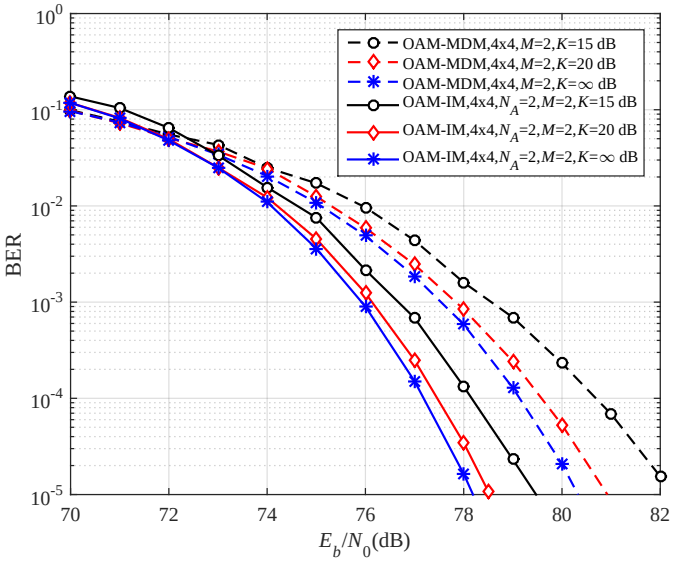

Fig. 7. OAM-IM and OAM-MDM comparison for Rician fading channels.

between transmit and receive UCAs, in which the plane of receive UCA is tilted towards the plane of transmit UCA with an angle of δ. This results in the violation of the orthogonality of OAM modes and creates inter-mode interference. For this case, the distance between the corresponding antenna elements can be calculated after tedious trigonometric calculations as

$$d_{np}^{\delta} = \sqrt{\tilde{d}^2 + r_{\text{tx}}^2 + \tilde{r}^2 - 2\tilde{r}r_{\text{tx}}\cos\phi_{np}} \tag{25}$$

where $\tilde{d} = d - r_{\text{rx}}\cos\phi_p \sin\delta$, $r = r_{\text{rx}}(\cos^2\delta\sin^2\phi + \cos^2\phi)^{1/2}$, $\phi = \arctan(\frac{\cot\phi_p}{\cos\delta})$ and $\phi_p = 2\pi p/N$. As seen from Fig. 6, both 4×4 OAM-MDM and OAM-IM schemes are quite sensitive to the tilt angle of the receive UCA; however, we also observe that OAM-IM scheme is more robust to imperfect alignment.

Although OAM literature generally assumes free-space LOS propagation, in order to observe the effects of non-LOS (NLOS) components, we consider a Rician fading channel model by characterizing the wireless channel with

$$\mathbf{H} = \sqrt{\frac{K}{K+1}}\mathbf{H}_{\text{LOS}} + \sqrt{\frac{1}{K+1}}\mathbf{H}_{\text{NLOS}} \tag{26}$$

where K is the Rician factor and $\mathbf{H}_{\text{LOS}}$ is the LOS channel matrix that was defined in Section II. The effect of NLOS components is captured by $\mathbf{H}_{\text{NLOS}}$, whose entries follow $\mathcal{CN}(0, L^2)$ distribution, where in accordance with (7), we consider $L = \lambda/(4\pi d)$ to account for the path loss. For this case, $\mathbf{\Lambda}$ of (10) has also non-zero off-diagonal elements, which ruin the orthogonality of OAM modes and we assume that the receiver has no knowledge of $\mathbf{H}_{\text{NLOS}}$. In Fig. 7, the effects of NLOS components are investigated with different K values for 4×4 OAM-IM and OAM-MDM schemes. As seen from Fig. 7, the performance of both OAM-MDM and OAM-IM schemes degrades with decreasing Rician K factors; however, we also observe that OAM-IM is more robust to the effects of NLOS components compared to the OAM-MDM scheme.

VI. Conclusions

In this paper, we have introduced the concept of OAM-IM as a potential candidate for next-generation short-distance wireless networks. More specifically, we have considered a new dimension, orthogonal OAM modes, for the emerging IM applications. The potential of the OAM-IM scheme, which has been proved by theoretical BEP derivations as well as computer simulations, has shown that IM-based solutions can provide improvements for also non-fading communication scenarios. Our future work may focus on the enhancement/generalization of OAM-IM and possible real-time experiments.

References

[1] *Draft new Report ITU-R M.[IMT-2020.TECH PERF REQ] - Minimum requirements related to technical performance for IMT-2020 radio interface(s)*, Feb. 2017. [Online]. Available: https://www.itu.int/md/R15-SG05-C-0040/en

[2] F. Tamburini, E. Mari, A. Sponselli, B. Thide, A. Bianchini, and F. Romanato, "Encoding many channels on the same frequency through radio vorticity: First experimental test," *New J. Phys.*, vol. 14, no. 3, p. 033001, Mar. 2012.

[3] A. E. Willner, "Communication with a twist," *IEEE Spectrum*, vol. 53, no. 8, pp. 34–39, Aug. 2016.

[4] D. Lee, H. Sasaki, H. Fukumoto, K. Hiraga, and T. Nakagawa, "Orbital angular momentum (OAM) multiplexing: An enabler of a new era of wireless communications," *IEICE Trans. Commun.*, vol. E100.B, no. 7, pp. 1044–1063, July 2017.

[5] S. M. Mohammadi, L. K. S. Daldorff, J. E. S. Bergman, R. L. Karlsson, B. Thide, K. Forozesh, T. D. Carozzi, and B. Isham, "Orbital angular momentum in radio–A system study," *IEEE Trans. Antennas Propag.*, vol. 58, no. 2, pp. 565–572, Feb. 2010.

[6] O. Edfors and A. J. Johansson, "Is orbital angular momentum (OAM) based radio communication an unexploited area?" *IEEE Trans. Antennas Propag.*, vol. 60, no. 2, pp. 1126–1131, Feb. 2012.

[7] K. A. Opare and Y. Kuang, "Performance of an ideal wireless orbital angular momentum communication system using multiple-input multiple-output techniques," in *2014 Int. Conf. on Telecommun. and Multimedia (TEMU)*, Heraklion, Greece, July 2014, pp. 144–149.

[8] A. Haskou, P. Mary, and M. Helard, "Error probability on the orbital angular momentum detection," in *2014 IEEE 25th Ann. Int. Symp. on Personal, Indoor, and Mobile Radio Commun. (PIMRC)*, Washington, DC, USA, Sept. 2014, pp. 302–307.

[9] E. Cano, B. Allen, Q. Bai, and A. Tennant, "Generation and detection of OAM signals for radio communications," in *2014 Loughborough Antennas and Propag. Conf. (LAPC)*, Loughborough, UK, Nov. 2014, pp. 637–640.

[10] K. A. Opare, Y. Kuang, J. J. Kponyo, K. S. Nwizege, and Z. Enzhan, "The degrees of freedom in wireless line-of-sight OAM multiplexing systems using a circular array of receiving antennas," in *2015 5th Int. Conf. on Advanced Comput. Commun. Technol.*, Haryana, India, Feb. 2015, pp. 608–613.

[11] K. A. Opare, Y. Kuang, and J. J. Kponyo, "Mode combination in an ideal wireless OAM-MIMO multiplexing system," *IEEE Wireless Commun. Lett.*, vol. 4, no. 4, pp. 449–452, Aug. 2015.

[12] Y. Yuan, Z. Zhang, J. Cang, H. Wu, and C. Zhong, "Capacity analysis of UCA-based OAM multiplexing communication system," in *2015 Int. Conf. on Wireless Commun. Signal Process. (WCSP)*, Nanjing, China, Oct. 2015, pp. 1–5.

[13] D. K. Nguyen, O. Pascal, J. Sokoloff, A. Chabory, B. Palacin, and N. Capet, "Antenna gain and link budget for waves carrying orbital angular momentum," *Radio Sci.*, vol. 50, no. 11, pp. 1165–1175, Nov. 2015.

[14] H. Tian, Z. Liu, W. Xi, G. Nie, L. Liu, and H. Jiang, "Beam axis detection and alignment for uniform circular array-based orbital angular momentum wireless communication," *IET Commun.*, vol. 10, no. 1, pp. 44–49, Feb. 2016.

[15] L. Sung, D. Park, and D. h. Cho, "Performance analysis of orbital angular momentum (OAM) transmission using dual polarization antenna based uniform circular array architecture," in *2016 13th IEEE Ann. Consumer Commun. Netw. Conf. (CCNC)*, Las Vegas, NV, USA, Jan. 2016, pp. 517–522.

[16] W. Zhang, S. Zheng, Y. Chen, X. Jin, H. Chi, and X. Zhang, "Orbital angular momentum-based communications with partial arc sampling receiving," *IEEE Commun. Lett.*, vol. 20, no. 7, pp. 1381–1384, July 2016.

[17] Y. Hu, S. Zheng, Z. Zhang, H. Chi, X. Jin, and X. Zhang, "Simulation of orbital angular momentum radio communication systems based on partial aperture sampling receiving scheme," *IET Microw. Antennas Propag.*, vol. 10, no. 10, pp. 1043–1047, July 2016.

[18] W. Zhang, S. Zheng, X. Hui, R. Dong, X. Jin, H. Chi, and X. Zhang, "Mode division multiplexing communication using microwave orbital angular momentum:An experimental study," *IEEE Trans. Wireless Commun.*, vol. 16, no. 2, pp. 1308–1318, Feb. 2017.

[19] Y. Ren, L. Li, G. Xie, Y. Yan, Y. Cao, H. Huang, N. Ahmed, Z. Zhao, P. Liao, C. Zhang, G. Caire, A. F. Molisch, M. Tur, and A. E. Willner, "Line-of-sight millimeter-wave communications using orbital angular momentum multiplexing combined with conventional spatial multiplexing," *IEEE Trans. Wireless Commun.*, vol. 16, no. 5, pp. 3151–3161, May 2017.

[20] Z. Zhang, Y. Yuan, J. Cang, H. Wu, and X. Zhang, "An orbital angular momentum-based in-band full-duplex communication system and its mode selection," *IEEE Commun. Lett.*, vol. 21, no. 5, pp. 1183–1186, May 2017.

[21] C. Zhang and L. Ma, "Trellis-coded OAM-QAM union modulation with single-point receiver," *IEEE Commun. Lett.*, vol. 21, no. 4, pp. 690–693, Apr. 2017.

[22] E. Basar, "Index modulation techniques for 5G wireless networks," *IEEE Commun. Mag.*, vol. 54, no. 7, pp. 168–175, June 2016.

[23] M. Di Renzo, H. Haas, A. Ghrayeb, S. Sugiura, and L. Hanzo, "Spatial modulation for generalized MIMO: Challenges, opportunities, and implementation," *Proc. IEEE*, vol. 102, no. 1, pp. 56–103, Jan. 2014.

[24] E. Basar, U. Aygolu, E. Panayirci, and H. V. Poor, "Orthogonal frequency division multiplexing with index modulation," *IEEE Trans. Signal Process.*, vol. 61, no. 22, pp. 5536–5549, Nov. 2013.

[25] E. Basar and I. Altunbas, "Space-time channel modulation," *IEEE Trans. Veh. Technol.*, vol. 66, no. 8, pp. 7609–7614, Aug. 2017.

[26] P. Yang *et al.*, "Single-carrier SM-MIMO: A promising design for broadband large-scale antenna systems," *IEEE Commun. Surveys Tuts.*, vol. 18, no. 3, pp. 1687–1716, 3rd Quart. 2016.

[27] P. Yang, Y. Xiao, Y. L. Guan, Z. Liu, S. Li, and W. Xiang, "Adaptive SM-MIMO for mmWave communications with reduced RF chains," *IEEE J. Sel. Areas Commun.*, vol. 35, no. 7, pp. 1472–1485, July 2017.

[28] P. Yang, Y. Xiao, S. Li, and L. Hanzo, "A low-complexity power allocation algorithm for multiple-input-multiple-output spatial modulation systems," *IEEE Trans. Veh. Technol.*, vol. 65, no. 3, pp. 1819–1825, Mar. 2016.

[29] P. Yang, Y. L. Guan, Y. Xiao, M. Di Renzo, S. Li, and L. Hanzo, "Transmit precoded spatial modulation: Maximizing the minimum euclidean distance versus minimizing the bit error ratio," *IEEE Trans. Wireless Commun.*, vol. 15, no. 3, pp. 2054–2068, Mar. 2016.

[30] R. Mesleh, H. Elgala, and H. Haas, "Optical spatial modulation," *IEEE/OSA J. Optical Commun. Netw.*, vol. 3, no. 3, pp. 234–244, Mar. 2011.

[31] E. Basar and E. Panayirci, "Optical OFDM with index modulation for visible light communications," in *2015 4th Int. Workshop on Optical Wireless Commun.(IWOW)*, Istanbul, Turkey, Sept. 2015, pp. 11–15.

[32] A. Yesilkaya, E. Basar, F. Miramirkhani, E. Panayirci, M. Uysal, and H. Haas, "Optical MIMO-OFDM with generalized LED index modulation," *IEEE Trans. Commun.*, vol. 65, no. 8, pp. 3429–3441, Aug. 2017.

[33] G. Kaddoum, M. F. A. Ahmed, and Y. Nijsure, "Code index modulation: A high data rate and energy efficient communication system," *IEEE Commun. Lett.*, vol. 19, no. 2, pp. 175–178, Feb. 2015.

[34] E. Ozturk, E. Basar, and H. A. Cirpan, "Generalized frequency division multiplexing with index modulation," in *2016 IEEE Globecom Workshops (GC Wkshps)*, Washington DC, USA, Dec. 2016, pp. 1–6.

[35] J. Zhang, M. Zhao, J. Zhong, P. Xiao, and T. Yu, "Optimised index modulation for filter bank multicarrier system," *IET Commun.*, vol. 11, no. 4, pp. 459–467, Mar. 2017.

[36] E. Basar, M. Wen, R. Mesleh, M. D. Renzo, Y. Xiao, and H. Haas, "Index modulation techniques for next-generation wireless networks," *IEEE Access*, vol. 5, pp. 16 693–16 746, Sep. 2017.

Ertugrul Basar (S'09-M'13-SM'16) received the B.S. degree (Hons.) from Istanbul University, Turkey, in 2007, and the M.S. and Ph.D. degrees from Istanbul Technical University in 2009 and 2013, respectively. He spent the academic year 2011-2012 with the Department of Electrical Engineering, Princeton University, NJ, USA. He was an Assistant Professor with Istanbul Technical University from 2014 to 2017, where he is currently an Associate Professor of Electronics and Communication Engineering. He is an inventor of two pending patents on index modulation schemes. His primary research interests include MIMO systems, index modulation, cooperative communications, OFDM, and visible light communications.

Recent recognition of his work includes the Turkish Academy of Sciences Outstanding Young Scientist Award in 2017, the IEEE Turkey Research Encouragement Award in 2017, and the Istanbul Technical University Best Ph.D. Thesis Award in 2014. He is also the recipient of four Best Paper Awards including one from the IEEE International Conference on Communications 2016. He has served as a TPC member for several IEEE conferences and is a regular reviewer for various IEEE journals. Dr. Basar currently serves as an Associate Editor of IEEE COMMUNICATIONS LETTERS and IEEE ACCESS, and as an Editor of *Physical Communication (Elsevier).*